GPS Receiver Architectures and Measurements

MICHAEL S. BRAASCH, MEMBER, IEEE, AND A. J. VAN DIERENDONCK, SENIOR MEMBER, IEEE

Invited Paper

Although originally developed for the military, the Global Positioning System (GPS) has proven invaluable for a multitude of civilian applications. Each application demands specific performance from the GPS receiver, and the associated requirements often vary widely. This paper describes the architectures and functions of civilian GPS receivers and then focuses on performance considerations. The fundamental receiver measurements are described and the quality of these measurements are related to the aforementioned receiver architectures.

***Keywords*—** *Code division multiaccess, distance measurement, global positioning system, microwave receivers, phase locked loops, radio navigation, satellite navigation systems.*

I. INTRODUCTION

Beyond its original purpose as a military "force enhancer," the Global Positioning System (GPS) has proven to be a great asset in a variety of civilian applications. Aircraft navigation systems use GPS for more direct routing. Surveyors achieve millimeter-level accuracy, and the same techniques are exploited by geophysicists to monitor crustal deformation. Automotive applications include fleet management, in-car navigation systems, and automatic position reporting during emergency cellular phone calls. Mariners use GPS for low-visibility harbor operations as well as for navigation in open waters. Hand-held receivers are proving useful to hikers, campers, and other recreational users.

The demands on GPS receiver performance are as varied as the applications. For example, the hiker is not interested in millimeter-level positioning, but a compact, low-weight, long battery-life unit is highly desirable. Surveying units may take advantage of the increased accuracy which can be achieved by exploiting the low-level of dynamics of the receiver.

Although the specific requirements vary significantly, the most fundamental aspects remain unchanged. Every GPS application ultimately involves the determination of platform position, velocity, and/or time. The exact algorithms and implementations differ depending upon the application but in each case the most basic measurements are the same: user-to-satellite line-of-sight (LOS) range and range-rate. Information describing the satellite position and velocity is also required. This is transmitted to the user in the form of binary data over the ranging signal via a spread-spectrum communication technique [1], [2].

This paper has been structured to provide the reader with the concepts necessary to understand the GPS receiver architecture. We discuss how the measurements are formed and how the various error sources affect the quality of the data. The paper is organized as follows. Section II provides an overview of GPS signal processing. The fundamentals of spread spectrum are reviewed briefly followed by a conceptual description of the range and range-rate measurement process. Section III provides a functional description of the GPS receiver. This includes consideration of the front-end, downconversion, digitization, and baseband processing. The fundamental measurements are described and common variants of the generic receiver architecture are outlined. In Section IV, receiver performance is discussed. The impact of various architectures on measurement accuracy is highlighted along with the issues of data rates, latencies, and interference tolerance. Section V summarizes the paper and draws some general conclusions.

II. GPS SIGNAL PROCESSING

Although providing position, velocity, and time is the ultimate goal of GPS, when considered as a sensor, the receiver's primary tasks are measurement of range and range-rate and demodulation of the navigation data. The navigation data are the 50-bits/s data stream modulated onto the GPS signal. The navigation data contain the satellite clock and orbital parameters which are used in the computation of user position. The GPS signal format is known as direct sequence spread spectrum [1], [2]. More details on spread spectrum will be given in Section II-A. The focus of this paper is on the process of exploiting the GPS spread-spectrum signal in order to determine range and range-rate. First, a brief review of spread spectrum fundamentals is given. This is followed by a conceptual

Manuscript received June 17, 1997; revised September 1, 1998.

M. S. Braasch is with the Avionics Engineering Center, School of Electrical Engineering and Computer Science, Ohio University, Athens, OH 45701-2979 (e-mail: mbraasch@oucsace.cs.ohiou.edu).

A. J. Van Dierendonck is with A. J. Systems, Los Altos, CA 94024-4925 USA (e-mail: AJVD@aol.com).

Publisher Item Identifier S 0018-9219(99)00425-9.

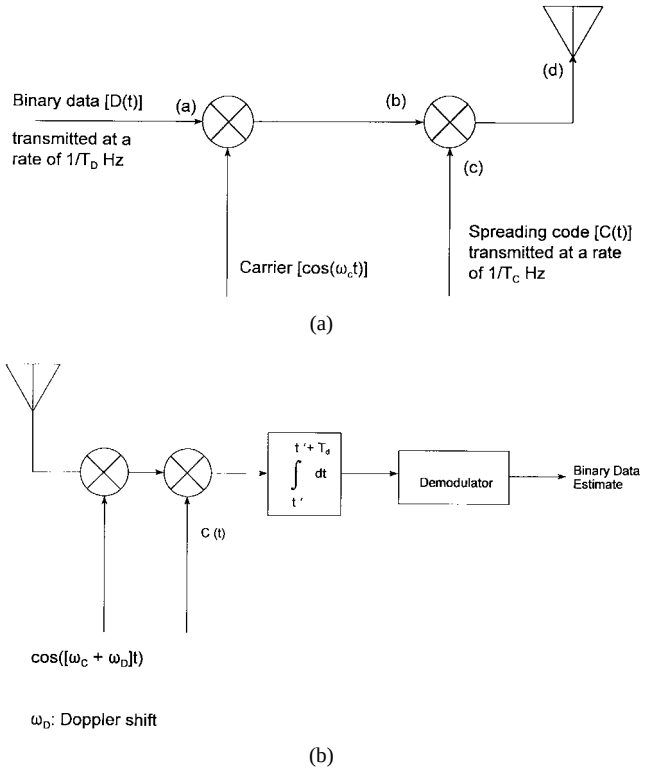

Fig. 1. (a) Simplified BPSK DSSS transmitter block diagram. Points (a), (b), (c), and (d) correspond to the signals given by the same letters in Fig. 2. (b) Simplified BPSK DSSS receiver block diagram. Mixing of the locally generated carrier brings the signal down to baseband. Mixing of the locally generated prn code $c(t)$ plus the subsequent integration together act as a correlation function.

description of how the GPS spread-spectrum signal is exploited to determine range and range-rate.

A. Spread-Spectrum Fundamentals

A spread-spectrum system [1], [2] typically is distinguished by the following three characteristics: 1) the data are modulated onto the carrier such that the transmitted signal has a larger (and usually much larger) bandwidth than the information rate of the data, hence the name "spread spectrum"; 2) a deterministic signal, known *a priori* to the receiver, is used by the transmitter to modulate the information signal and spread the spectrum of the transmitted signal; and 3) the receiver cross correlates the received signal with a copy of the deterministic signal in the process of demodulating the data. By so doing, the receiver can recover the transmitted data.

The type of spread spectrum employed by GPS is known as binary phase shift keying direct sequence spread spectrum (BPSK DSSS). The term "direct sequence" is used when the spreading of the spectrum is accomplished by phase modulation of the carrier. BPSK is the simplest form of phase modulation where the carrier is instantaneously phase shifted by 180° at the time of a bit change.

Consider the simplified block diagrams of a BPSK DSSS transmitter and coherent receiver depicted in Fig. 1(a) and (b). The binary data in the form of analog voltages either at $+1$ or -1 is input at a rate of $1/T_D$ bits/s. The modulation of the binary data onto the carrier may be considered as a simple mixing operation; the same is true for the modulation of the spreading code which increases the bandwidth of the transmitted signal by a factor of T_D/T_C, where $T_D \gg T_C$ and $1/T_C$ is the spreading code rate. Fig. 2 provides time and frequency plots of the signals corresponding to points (a), (b), (c), and (d) in Fig. 1(a). The binary data/signal to be transmitted is plotted in Fig. 2(a). The result of the BPSK modulation of this data onto a carrier is plotted in Fig. 2(b), the spreading code is given in Fig. 2(c), and the transmitted signal is given in Fig. 2(d).

The coherent BPSK DSSS receiver [Fig. 1(b)] despreads the received signal by mixing in a copy of the spreading code and then integrating over a data bit period T_D. Since the data and spreading code have been modulated onto a carrier, the received signal must also be downconverted through mixing and filtering. This process leaves the binary data intact and thus, standard BPSK demodulation techniques can be applied. The despreading procedure, in general, is successful only if the receiver's locally generated copy of the spreading code is synchronized with the spreading code component of the received signal. Two questions thus arise. 1) How does the receiver know that its locally generated spreading code is synchronized (i.e., "locked") with the incoming code? 2) How does the receiver maintain lock?

The lock detector is formed by exploiting the correlation properties of the spreading code. In order to appreciate the spreading code correlation properties, first consider an infinite sequence of truly random bits. Note the spreading code "bits" are referred to as "chips." First, the autocorrelation function is defined as [2]

$$R_c(\tau) = \lim_{A\to\infty} \frac{1}{2A} \int_{-A}^{A} c(t)c(t-\tau)\,dt. \tag{1}$$

The autocorrelation of an infinite random sequence then is given by [2]

$$\begin{aligned} R(\tau) &= 1 - |\tau|, \qquad \text{for } |\tau| \le T_C \\ &= 0, \qquad \text{otherwise} \end{aligned} \tag{2}$$

where τ is the lag value in units of seconds.

A truly random chip sequence is not realizable in practice, but maximal-length sequences (m-sequences) provide a close approximation. An n-element shift register can generate an m-sequence of length N chips, where $N = 2^{\mathrm{n}} - 1$. The periodic autocorrelation function of an m-sequence is given by

$$\begin{aligned} R(\tau) &= 1 - |\tau|\left(\frac{1}{N} + 1\right), \qquad \text{for } |\tau| \le T_C \\ &= -\frac{1}{N}, \qquad \text{for } T_C \le |\tau| \le (N-1)T_C. \end{aligned} \tag{3}$$

Fig. 3 depicts the autocorrelation functions for the random and m-sequences. Spreading codes are usually formed from one or more m-sequences. Since the spreading codes approximate the properties of truly random sequences, they

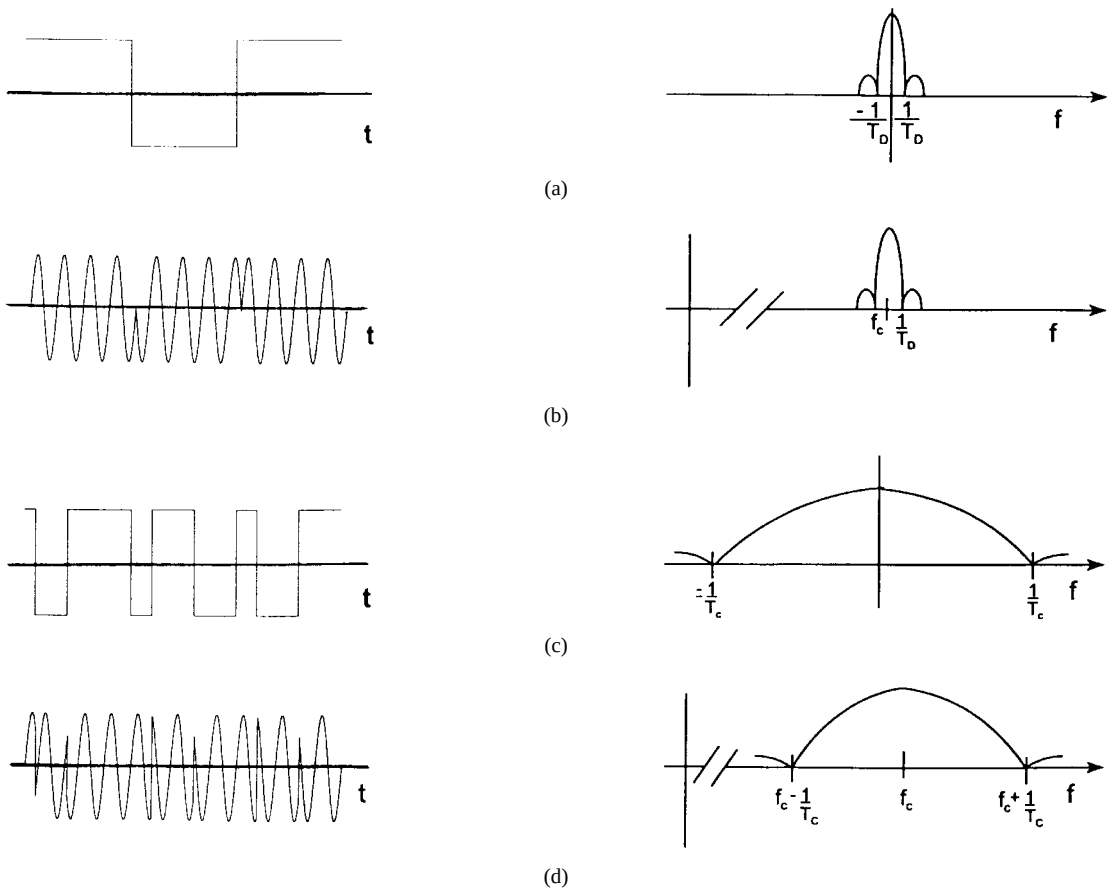

Fig. 2. Time and frequency plots for (a) data signal, (b) data BPSK modulated onto the carrier, (c) spreading code, and (d) spreading code modulated onto the data modulated carrier. Signals (a), (b), (c), and (d) are marked in Fig. 1(a) as well.

are referred to as pseudonoise (pn) or pseudorandom noise (prn) sequences. When the locally generated code is locked to the received code, the correlation effectively amplifies the underlying BPSK data signal. The amplification factor is given by N, the length of the prn sequence. The nonencrypted portion of the GPS signal employs spreading codes known as Gold codes [3]. The Gold codes are formed by combining two m-sequences. The result is a family of prn codes with low cross correlation between codes. This allows all satellites to transmit on the same carrier frequency without incurring significant mutual interference. The encrypted portion of the GPS signal also uses quasi-orthogonal codes, but they are not Gold codes [4], [5]. Since each satellite is assigned a unique code, the system is referred to as code-division multiple access (CDMA).

The spreading code lock detector may now be described. Based on the autocorrelation function of the m-sequence, it is apparent that the output of the integration block in the coherent receiver of Fig. 1(b) will be small if the locally generated code is not locked to the incoming code. On the other hand, a relatively large value will be achieved if the local and incoming codes are close to synchronization.

Once lock has been achieved, how is it maintained? Consider the case where the locally generated code is one-quarter chip early. The receiver thus is not quite locked. The normalized output of the integrator in Fig. 1(b) would be 3/4 rather than the maximum value of one. The same value would have been obtained had the local code been generated one-quarter chip late rather than early. A prn code phase detector, also known as a discriminator function, is required. This discriminator must have an output that is unambiguous with respect to the sign of the local code delay. This typically is achieved by correlating the received signal with multiple versions of the locally generated code. Consider the correlation function associated with a local code purposely generated $d/2$ chip early and the correlation function with a local code $d/2$ chip late, $d \leq 1$. A discriminator function may be formed by differencing the early and late correlation functions (see Fig. 4). Lock may be maintained by feeding back the output of the discriminator to the local code generator such that the discriminator output is driven to zero. This mechanization is referred to as the delay-lock loop (DLL).

The lock-detector, described earlier, allows the receiver to determine if the local code is being generated within ± 1 chip of the received code. The initial acquisition of a satellite signal involves two parts. One is a search over all possible shifts of the locally generated code relative to the received code. Second, as with any superheterodyne receiver, is the mixing of a locally generated carrier signal with the incoming signal. The despreading and data demodulation process is successful only if the locally

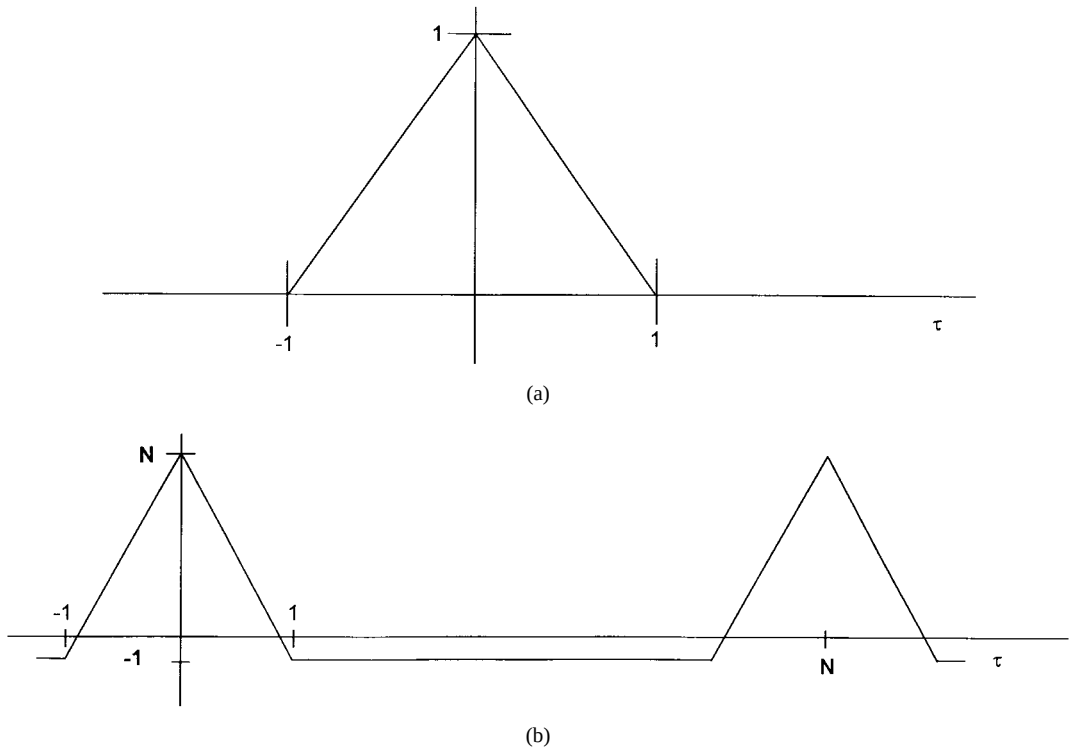

Fig. 3. Autocorrelation functions of (a) normalized autocorrelation function of an infinite-length, truly random chip sequence and (b) autocorrelation function of a finite-length (N chips), maximal length sequence.

generated carrier is either frequency or phase locked to the received carrier. Satellite and user vehicle dynamics-induced Doppler shifts and satellite frequency reference inaccuracies all contribute to a shift in the received carrier frequency. Inaccuracies in the receiver frequency reference also add uncertainty as a result of signal downconversion in the front end. The acquisition process thus consists of a search for both prn code shift and local carrier frequency offset. Finally, just as a delay-lock loop is required to maintain lock on the received prn code, a frequency-lock loop (FLL) or phase-lock loop (PLL) is required to maintain lock on the received carrier.

With this brief overview of spread spectrum fundamentals, we may now discuss the concept of spread-spectrum ranging.

B. The Concepts of Pseudorange, Delta Range, and Accumulated Delta Range

This section will describe the fundamental ranging measurements formed in a GPS receiver. A detailed description of receiver operations is given in a later section.

1) Pseudorange: Consider a signal being generated and transmitted by a GPS satellite. Through precise modulation of the carrier, the satellite effectively time stamps the signal as it is being transmitted. The time at which the signal was transmitted is thus an integral part of the signal itself. The signal transits from the satellite to the user and thus is received at a later time. The time stamp on the signal, also known as the time of transmission (TOT), is then decoded by the receiver. In this simplified example, the satellite-to-user range is given by $R = c^*(\text{TOR} - \text{TOT})$, where c is the speed of light and TOR is the time of reception of the signal at the receiver.

The TOT is encoded onto the broadcast signal in two parts. A coarse time stamp is included as part of the binary data transmitted with the GPS signal. A fine adjustment is achieved by tracking the prn code component of the signal. The prn code is generated at a fixed, known rate. By tracking the received prn code, the receiver is tracking inherently the time at which the signal was transmitted, thus TOT [16].

It is important to recognize that the range measurement just described only works properly if the satellite and receiver clocks are synchronized. This is never the case. The difference between the observed TOT and TOR is thus a function of both satellite-to-receiver range and receiver clock offset. Specifically

$$PR = c * (\text{TOR} - \text{TOT}) = R + c * b \qquad (4)$$

where R is the satellite-to-user range, b is the receiver clock offset (usually referred to as the clock bias), and PR is the resulting range-like observable known as the pseudorange. In reality, the raw pseudorange measurement also contains a satellite clock offset from GPS system time. This can be corrected, however, using parameters transmitted to the user via the navigation data message. As is described more fully in [6], the process of positioning requires pseudorange measurements to four satellites at a minimum. The navigation solution involves the simultane-

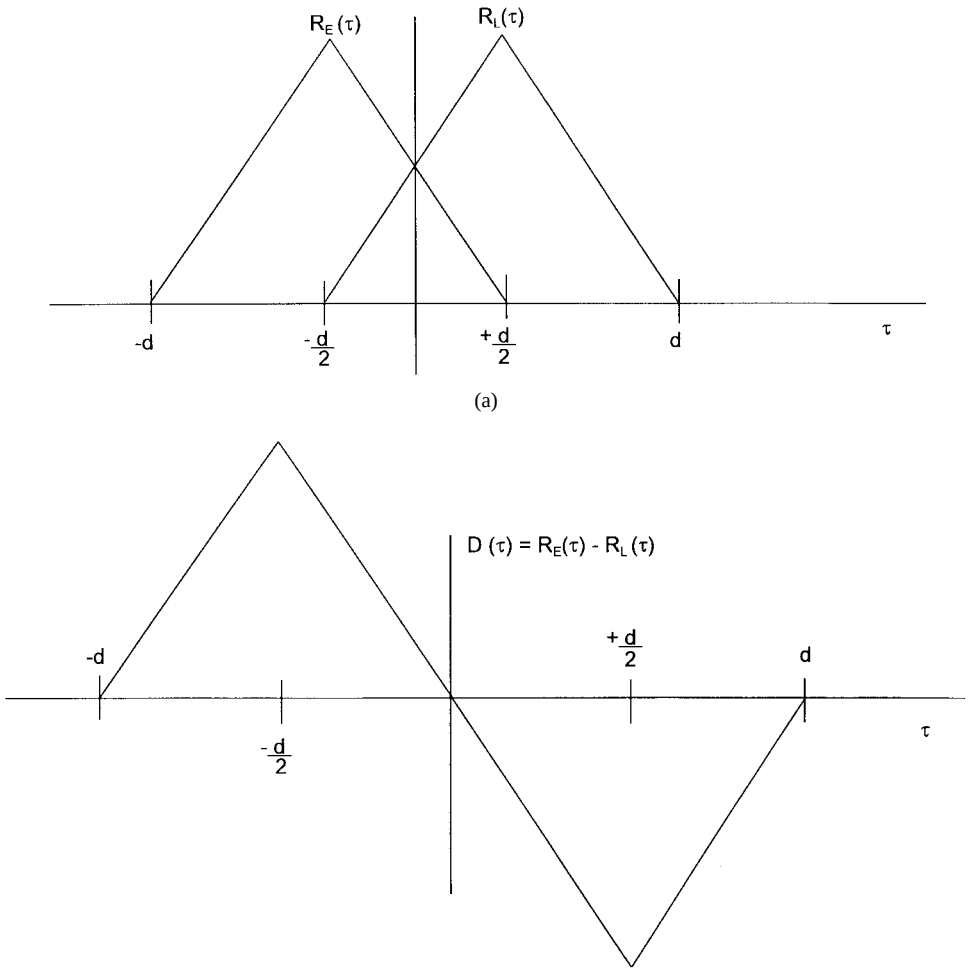

Fig. 4. (a) Cross-correlation functions between the received code and locally generated codes which are $d/2$ chip early and late and (b) code-phase discriminator function formed from the difference between the correlation functions in (a).

ous solution of four unknowns: three-dimensional position of the antenna/receiver and the receiver clock bias.

2) Delta Range and Accumulated Delta Range: Conceptually, the determination of range rate is straightforward. The receiver tracks the Doppler-shifted carrier either with an FLL or a PLL. The Doppler shift of electromagnetic waves is given approximately by

$$f_R \approx f_o\left(1+\frac{v_{los}}{c}\right) \tag{5}$$

where f_o is the transmitted frequency, f_R is the received frequency, v_{los} is LOS velocity, and c is the speed of light. Note that due to the convention used in the equation, v_{los} is negative if the transmitter-to-receiver range is increasing. From (5), LOS velocity is given by

$$v_{los} \approx c\left(\frac{f_R}{f_o}-1\right) \tag{6}$$

and in terms of the Doppler shift $f_D = f_R - f_o$

$$v_{los} \approx c\left(\frac{f_D}{f_o}\right). \tag{7}$$

Finally, the wavelength of the transmitted carrier is given by $\lambda_o = c/f_o$, thus

$$v_{los} \approx \lambda_o f_D. \tag{8}$$

Thus, average LOS velocity may be formed by simply counting the number of Doppler cycles over a short period (e.g., 0.1 s) and then scaling by the wavelength and dividing by the duration of the integration interval. In many military receivers, an FLL is used to form the velocity estimate, and the result is referred to as the delta-range measurement.

Alternately, accumulated delta range (i.e., change of range) is formed if the Doppler count is kept running continuously. By continuously running the accumulation, (8) is being integrated. The integral of velocity is, of course, displacement or change of range relative to the start of the integration. At the end of a given integration interval, a whole number of Doppler cycles will have been counted, but usually a fraction of a cycle would remain. If this fractional phase is also measured and included in the accumulated delta-range observable, it is also referred to as an "integrated Doppler" or "carrier phase" measurement.

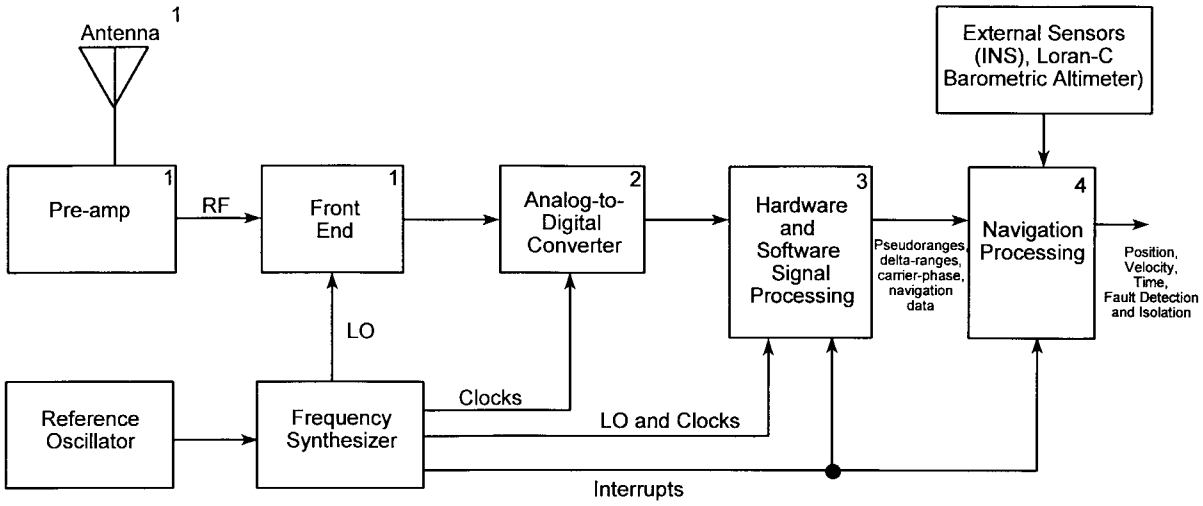

Fig. 5. Generic GPS receiver block diagram. 1) Antenna/Front-End: single-frequency designs pass the L1 (1575.42-MHz) signal only; dual-frequency designs pass both the L1 and L2 (1227.6-MHz) signals. 2) Analog-to-Digital (A/D) Converter: several types may be found in current receivers, such as single-bit (i.e., hard limiting), multibit, and adaptive threshold types. 3) Hardware/Software Signal Processing: single-channel designs sequentially process each satellite being tracked; multichannel designs multiplex the A/D output into parallel channels with each channel tracking separate satellites. 4) Navigation Processing: integration of GPS and external sensor data may occur outside the GPS receiver.

As will be shown later, the tracking accuracy of the carrier phase measurement can be as small as a millimeter. Unfortunately, it is only a measure of the change in satellite-to-receiver range relative to the time the accumulation was started. The carrier phase is thus an ambiguous measure of range. The pseudorange is not ambiguous but the tracking accuracy is on the order of a meter. The precision of the carrier phase measurements can be exploited in differential positioning as is described by Herring [7] in this issue. In addition, the carrier phase measurements can be used to filter the noise in the pseudorange, thereby improving accuracy through a process known as carrier smoothing [8], [43].

III. Receiver Architecture Overview

Attention will now be given to the actual receiver operation. A block diagram of a generic GPS receiver is given in Fig. 5.

A. Antenna and Preamplifier

The antenna normally is right-hand circularly polarized to match the incoming signal, and the pattern is essentially hemispherical in most applications. This pattern allows tracking of satellites from zenith almost down to the horizon for all azimuths. A wide variety of antennas exist. The most common is a low-profile type consisting of a microstrip patch element. Other types include helixes and variants such as the quadrafilar helix. Phased arrays originally were used exclusively by the military for jammer-nulling. Now, however, civilian applications of the array concept include multipath rejection [44]. Another common multipath-reducing design is the so-called "choke ring" in which the antenna is located in the middle of a set of concentric electrically-conducting rings. Low-elevation angle signals are nulled by the rings, and thus the antenna's gain effectively is reduced at these low angles [9].

Following the antenna, the pre-amplifier sets the noise figure for the entire receiver system and typically has a gain on the order of 25–40 dB. Typical low-noise amplifiers have noise figures less than 2 dB, but the addition of preselection filtering, burnout protection, and other associated losses usually result in an overall noise figure of 3–4 dB.

B. Front End

The analog signal processing involves filtering, amplification, and downconversion. Given the low power of the received signal, out-of-band interference must be suppressed using sharp cutoff filters. This is often accomplished using surface acoustic wave (SAW) devices. Amplification is straightforward in hard-limiting architectures (1-bit A/D conversion) but multibit receivers must employ some form of automatic gain control (AGC). Downconversion is performed either in single or multiple stages. Multistage architectures allow for adequate image suppression and general bandpass filtering with the final intermediate frequencies (IF's) placed close to baseband (e.g., 4 MHz). Single-stage downconversion is becoming more prevalent, however, and image suppression is achieved by accepting a higher IF (e.g., 30–100 MHz). The final conversion to baseband involves converting the IF signal to the in-phase (I) and quadrature (Q) components of the signal envelope [10]. This is accomplished by mixing the IF signal with two tones generated at the final nominal IF but with one tone lagging the other in phase by $\pi/2$ radians. The output of the two mixers are the baseband components plus the residual Doppler. This conversion to baseband can be accomplished either before or after A/D conversion.

Table 1
Satellite to Receiver Link Budget

Minimum Transmitted Signal Power (P)	26.8 dBW (transmit antenna gain included)
Free-Space Loss (F)	182.4 dB
Atmospheric Attenuation (A)	2.0 dB
Minimum Received Signal Power (S=P-F-A)	-157.6 dBW

An important signal quality metric, signal-to-noise ratio (SNR), will be discussed next. The bandwidth of the final stage of IF filtering ranges from 2 MHz in low-end receivers up to 20 MHz in high-performance models. The noise power in this bandwidth can be approximated by

$$N = kT_E B \tag{9}$$

where k is Boltzmann's constant (1.3806×10^{-23} JK^{-1}), B is the bandwidth in Hz, and T_E is the effective noise temperature in kelvin. The effective noise temperature is a function of sky noise, antenna noise temperature, line losses, receiver noise factor, and the ambient temperature. The ambient temperature and equipment noise factors are dominant and a typical effective noise temperature for a GPS receiver is 513 K. This results in noise power of approximately -138.5 dBW in a 2 MHz bandwidth (noise density: -201.5 dBW/Hz).

The next step in the process is to determine the signal power. The GPS link budget may be analyzed starting with the minimum power transmitted by the satellites. The C/A-code (at the 1575.42 MHz carrier frequency) is transmitted at an effective level of 478.63 W (26.8 dBW) effective isotropic radiated power (EIRP) [11], [12]. The actual satellite antenna is composed of a phased array which directs the signal in an approximately 29° beam toward the Earth. The average satellite-to-user distance for near-Earth users is approximately 2×10^7 m. The signal loses power density due to spherical spreading as it propagates and the free-space loss factor quantifies this phenomenon

$$\text{free-space loss factor} = \left(\frac{\lambda}{4\pi R}\right)^2 \tag{10}$$

where λ is the carrier wavelength (0.19 m at 1575.42 MHz) and R is the transmitter-to-receiver distance. Taking R as 2×10^7 m, the free-space loss factor is approximately 5.73×10^{-19} or -182 dB. Atmospheric attenuation is assumed to be approximately 2.0 dB [14] and thus the link budget is given in Table 1 (receiving antenna is assumed to be isotropic).

For more details on the satellite architecture and link budget, the reader is referred to [13]. The link budget just presented is in agreement with the GPS interface control document [14] which specifies a minimum signal level of -160 dBW. In a 2 MHz bandwidth, then, the C/A-code SNR is

$$\begin{aligned}\text{SNR} &= \text{Signal power in dB} - \text{Noise power in dB} \\ &= -157.6 - (-138.5) = -19.1 \text{ dB}.\end{aligned}$$

A sample plot of a raw digitized GPS signal-plus-noise is given in Fig. 6(a). The signal from a GPS antenna was amplified, filtered, and digitized directly at RF (for experimentation purposes) at a rate of approximately 5 MHz [15]. As expected from the SNR computation, only white noise is distinguishable. This is further evidenced by examining the fast Fourier transform (FFT) of the signal [Fig. 6(b)] and noting the spectrum is fairly flat. The nonideal passband characteristic of the front-end filters prevents the spectrum from being perfectly flat. It is clear, however, that the noise is dominant. The spectrum of the GPS signals from the visible satellites is not apparent since it lies well below the noise floor. Section III-D will highlight the increase in SNR which results from the baseband processing. See Fig. 9 for the FFT which results after demodulation (i.e., postcorrelation).

C. A/D Conversion

As was mentioned earlier, both single-bit and multibit architectures are currently in use. Most low-cost commercial receivers employ 1-bit sampling in narrow (i.e., 2-MHz) bandwidths. High-end receivers typically use anywhere from 1.5-bit (i.e., three levels) to 3-bit (eight levels) sampling in bandwidths ranging from 2–20 MHz. The signal transmitted by the satellite is filtered down to a bandwidth of 30 MHz. Although the main lobe, i.e., first-null bandwith of the C/A-code is a mere 2 MHz wide, better signal resolution and, subsequently, improved performance can be achieved if the receiver processes more than just the main lobe. More will be given on this later.

The degradation of the signal due to finite-bit quantization is dependent upon two factors in addition to the number of quantization levels [10]. First is the IF bandwidth. That is, the bandwidth of the final stage of the front end. Second is the ratio of the maximum A/D threshold to the rms noise level. One-bit sampling is a special case which does not depend upon the latter factor since there is only one threshold in this case and it is at zero. The degradations are listed in Table 2. The 1.96-dB degradation factor popularly applied to the 1-bit case is valid only for an infinite bandwidth signal. It should also be noted that the 3-bit results apply only when the automatic gain control in the front-end matches the input signal exactly to the dynamic range of the A/D converter.

The inherent tradeoffs must be emphasized. Following Nyquist, the required sampling rate is proportional to the IF bandwidth. Increased cost and complexity thus accompany the 3-dB improvement associated with the wideband processing. Finally, it should be noted that A/D converters with adaptive thresholds have been used to mitigate the effects of narrowband interference. This will be discussed further in a later section.

D. Baseband Signal Processing

Baseband processing of the digitized signal typically is accomplished using a combination of dedicated hardware (numerically controlled oscillators, correlators, accumulators) and digital signal processors (DSP's) to form the measurements and provide feedback for acquisition and

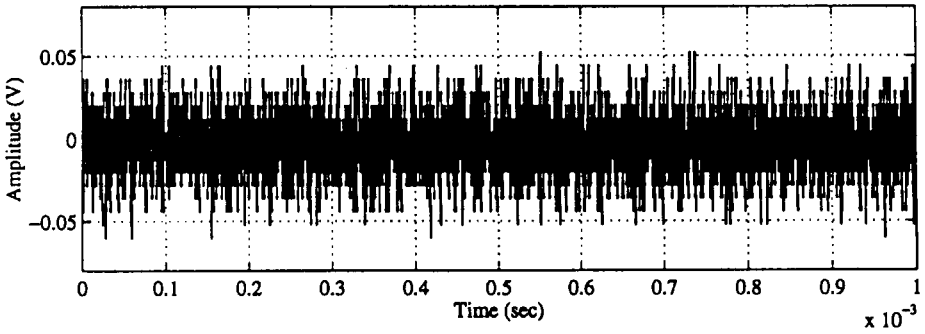

(a)

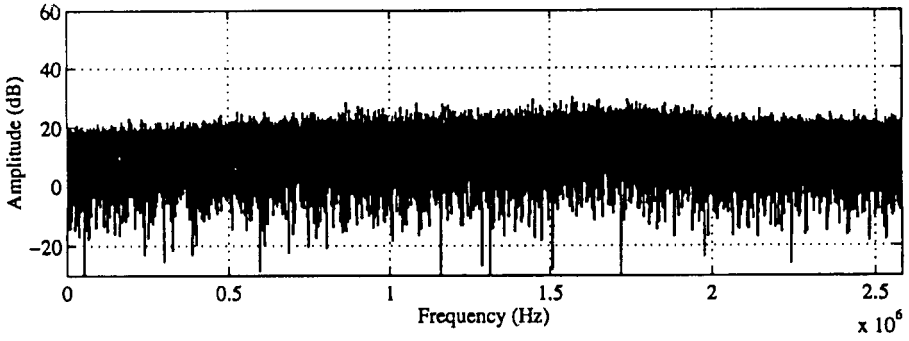

(b)

Fig. 6. (a) Time domain plot of raw GPS signal plus noise, sampled at approximately 5 MHz, after front-end processing (amplification and filtering only) and (b) magnitude of the precorrelation FFT of the GPS signals plus noise plotted in (a).

Table 2
Signal Degradation Due to Finite-Bit Quantization in the A/D Converter

	1-bit A/D converter	3-bit A/D converter
Narrow IF bandwidth ($1/T_C$ Hz)	3.5 dB	0.7 dB
Wide IF bandwidth ($5/T_C$ Hz)	2.25 dB	0.3 dB

tracking. The digitized samples are mixed with in-phase and quadrature outputs of the so-called carrier numerically controlled oscillator (NCO) to produce the I and Q data streams (Fig. 7). A feedback loop is used to ensure the NCO matches the phase or frequency of the received signal. This carrier NCO output also is accumulated to form the delta range and accumulated delta-range observables.

In addition to Doppler removal, the I and Q samples are mixed with early, prompt, and late versions of the prn code and then accumulated (i.e., filtered) to form the associated correlation values (recall the discussion on the DLL discriminator function in Section II-A). Prior to bit synchronization with the navigation data, the accumulation interval (i.e., predetection integration interval) typically is 1 ms (i.e., the length, in time, of one C/A-code). After bit synch, the accumulation interval typically is expanded to the duration of the navigation data bit (20 ms).

The prn code tracking is maintained through a feedback loop where the error signal is formed by differencing early and late correlation functions. Three common discriminators are as follows [10], [16]:

Coherent

$$D = (I_E - I_L)\text{sign}(I_P) \tag{11}$$

Early-minus-late power (noncoherent)

$$D = \left(I_E^2 + Q_E^2\right) - \left(I_L^2 + Q_L^2\right) \tag{12}$$

Dot-product (noncoherent)

$$D = (I_E - I_L)I_P + (Q_E - Q_L)Q_P \tag{13}$$

where I_E, I_L, I_P, Q_E, Q_L, and Q_P are defined in Fig. 7; sign (I_P) is the sign of the navigation message data bit. As indicated in Fig. 7, E, L, and P denote correlation with early, late, and prompt versions of the locally generated prn code. The three discriminator functions are plotted in Fig. 8.

The discriminator output is formed in the microprocessor and then filtered and scaled before being fed back to the code NCO (Fig. 7). Similarly, the I_P's and Q_P's are processed in the software PLL or FLL to demodulate the navigation data bits and provide feedback to the carrier NCO to maintain phase or frequency lock.

Traditional PLL's or FLL's and BPSK data-demodulation techniques can be applied since a positive SNR is achieved after despreading (i.e., correlation). Recall the signal in the front-end (i.e., after amplification and filtering) was

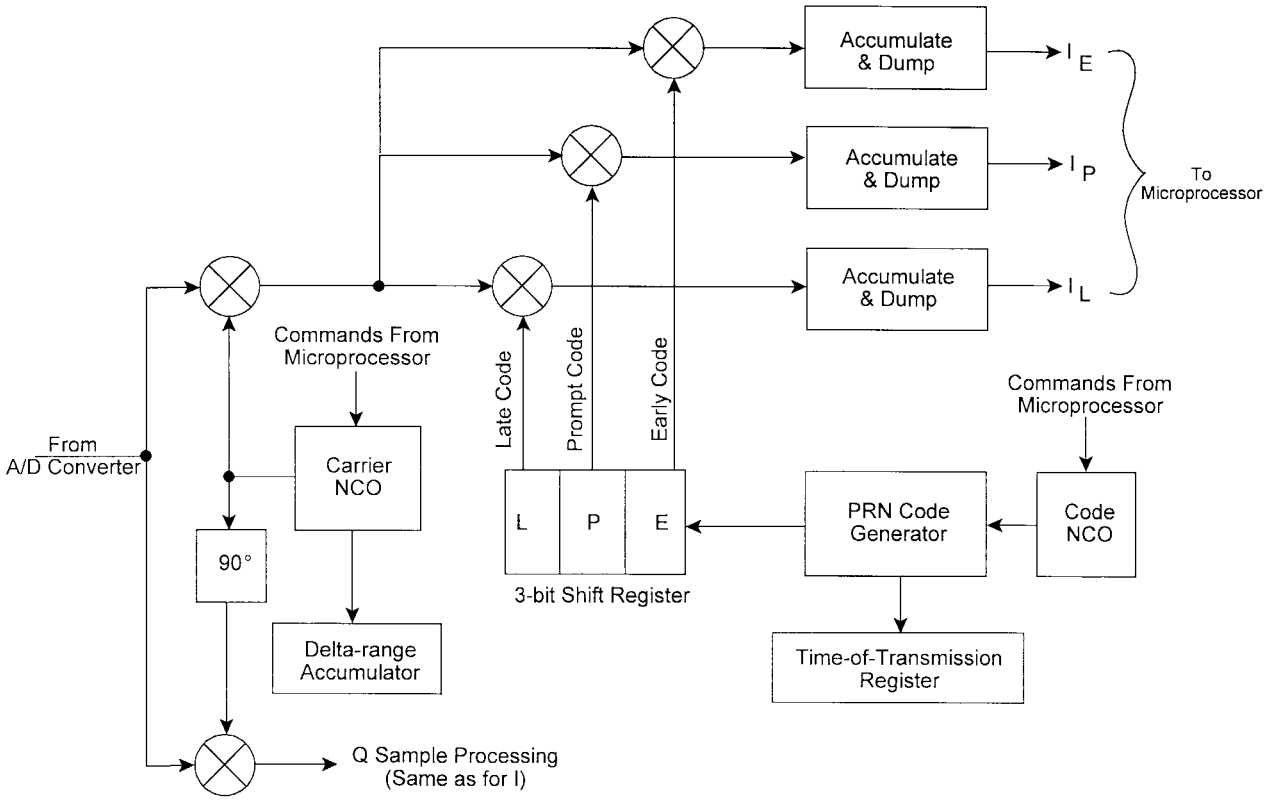

Fig. 7. Generic GPS baseband signal processing block diagram.

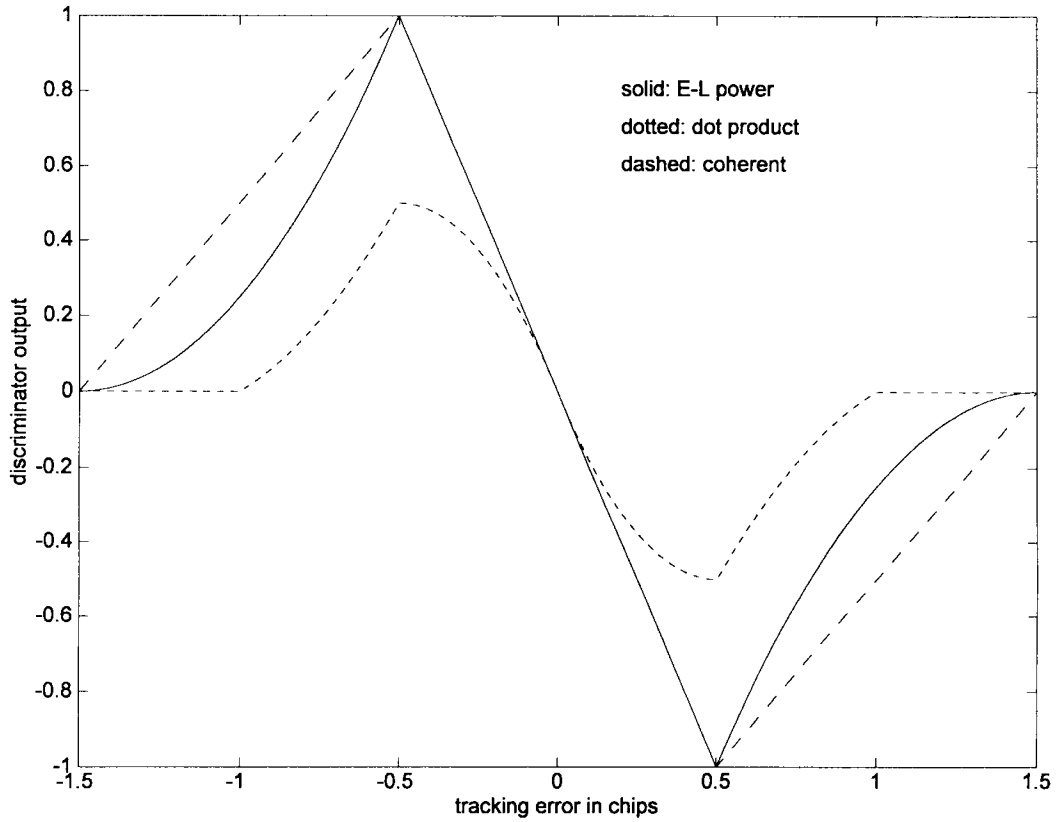

Fig. 8. Code-phase discriminator functions for three common DLL implementations.

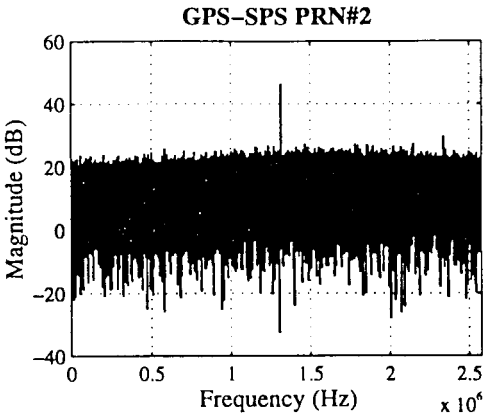

Fig. 9. Magnitude of the postcorrelation FFT of a GPS C/A signal present in the collected data plotted in Fig. 6(a).

completely buried in noise [Fig. 6(a) and (b)]. After being correlated with the locally generated code, however, the signal is despread thus occupying the bandwidth of the navigation data, namely, 50 Hz. Recalling the noise equation discussed earlier, the noise power in a 50-Hz bandwidth is approximately 3.54×10^{-19} W (-184.5 dBW). After correlation, and thus despreading, the SNR has increased to: SNR = Signal power in dB − Noise power in dB = $-157.6 - (-184.5) = +26.9$ dB. The increase in SNR as a result of despreading in this case is

$$\text{SNR gain} = 26.9 - (-19.1) = 46 \text{ dB}.$$

Recalling the front-end data presented in Fig. 6(a) and (b), Fig. 9 shows the computed spectra after the received signal was correlated with the C/A-code of a visible satellite [15]. The signal clearly has been raised above the noise floor thus allowing for tracking and measurement generation.

The SNR of spread-spectrum signals (like that of GPS) is a function of the point in the receiver under consideration. Precorrelation SNR's are negative whereas postcorrelation SNR's are positive. It is convenient, therefore, to normalize the SNR to a 1-Hz bandwidth and thus achieve a ratio of signal and noise which is bandwidth-independent. Alternately, this can be viewed as a density and the result is referred to as the "carrier-to-noise density" ratio

$$\text{C/N}_0 = (\text{SNR})(B) \text{ [ratio} - \text{Hz]} \tag{14}$$

where SNR is the straight ratio form of the SNR at a certain point in the receiver, say, the final IF stage, and B is the bandwidth (in Hz) of that stage of the receiver. Usually this quantity is converted into decibels

$$\text{C/N}_0 = 10 \log_{10}\{(\text{SNR})\ (B)\} \text{ [dB} - \text{Hz]}. \tag{15}$$

In both equations, the terms in square brackets denote the units in which C/N_0 is being expressed. The SNR in a 2-MHz bandwidth was approximately -19.1 dB (0.0123 in straight ratio) and $+26.9$ dB (490) in a 50-Hz bandwidth

$$\begin{aligned}\text{C/N}_0 &\approx 10 \log_{10}\left\{(0.0123)\,(2.046 \times 10^6)\right\} \\ &\approx 10 \log_{10}\{(490)\,(50)\} \approx 44 \text{ dB} - \text{Hz}.\end{aligned} \tag{16}$$

It should be recognized that this is merely a nominal figure. Received satellite signal power varies with user antenna gain, satellite elevation angle, and satellite age [5]. Typical C/N_0's range from 35–55 dB-Hz.

The GPS broadcast signal includes a C/A-code and P(Y)-code on the Link 1 (L1) frequency (1575.42 MHz) and a P(Y)-code on the L2 frequency (1227.6 MHz). The C/A-code is broadcast without encryption but the Y-code is an encrypted version of the P-code. The P-code was broadcast during the initial buildup of the GPS constellation, and many civilian receivers were built to track the P-code. However, after the full complement of satellites were in place in the early 1990's, the P-code was encrypted, thus forming the Y-code, and the Y-code has been broadcast since that time. Civilian receivers have been developed to track the Y-code and carrier on L1 or both L1 and L2 [17]–[20]. The Y-code has been deduced to be formed by combining the P-code with an unknown, lower-rate (approximately 500-kHz) prn code [17]–[20]. The civilian receivers treat the encryption code as high-rate data and essentially correlate with the underlying P-code during the span of each encryption prn code chip. The integration interval thus is reduced from the duration of a navigation data bit (1/50 s) to the duration of an encryption code chip (1/511 500 s). Without further modification, this would result in a tremendous noise penalty relative to C/A-code processing. However, rate-aiding from the C/A-code and carrier can be applied to the P(Y) channels allowing for significant narrowing of the tracking loop bandwidths and thus a minimization of the noise penalty.

IV. Performance Considerations

As indicated in Section I, receiver architectures vary significantly depending upon the intended application. This section will highlight the tradeoffs among the various architectures.

A. Acquisition

The process of acquiring the satellite signals involves multiple steps. Simultaneous searches of frequency and code offset are required followed by data bit synchronization, frame synchronization, and finally ephemeris and satellite clock data collection. This process is required for each satellite to be tracked. Multichannel architectures have dedicated hardware channels for each satellite and thus can perform the satellite searches in parallel. Although no longer in production, sequencing receivers are still in use today. Most are first-generation low-cost units. Sequencing receivers use temporal multiplexing in order to track more satellites than the number of available hardware channels. Such receivers are thus slower in the acquisition process. Acquisition times range from under 1 min up to 20 min depending upon the number of hardware channels available, the algorithms employed, and the signal/noise conditions.

Reacquisition is a related issue. This is the case where the receiver acquired the satellites but has lost lock temporarily. Short reacquisition times (i.e., on the order of seconds

or less) are especially critical in land-vehicle applications. In densely populated areas it is not uncommon to have more than 50% of the sky blocked by buildings. Even in less populated areas, trees and terrain can block satellites. Provided the blockage is on the order of a few seconds, modern receivers generally can reacquire in less than 15 s. The key parameter here is the maximum Doppler/receiver-clock uncertainty which the receiver can experience without having to revert to full acquisition mode. Doppler uncertainty is primarily a function of the dynamics of the platform on which the receiver/antenna is mounted since the satellite dynamics are known through the navigation data message. The receiver clock uncertainty (i.e., variation in clock frequency) is a function of the clock type and the environment (temperature, shock, vibration). High-end GPS receivers typically employ temperature-compensated crystal oscillators.

B. Tracking Accuracy

Measurement accuracy is limited by a variety of error sources. Most of the error sources have to do with the satellite or propagation medium and thus are not under the control of the receiver. Among these are satellite clock and ephemeris errors and atmospheric delays. However, sensitivity to thermal noise, interference, and multipath is highly dependent upon receiver architecture. Furthermore, the fact that these error sources are independent between spatially separated receivers makes them the dominant error sources in high precision differential applications [6].

1) Noise Performance: Closed-form expressions for DLL tracking error due to thermal noise have been derived under the assumption of infinite signal bandwidth [21]. We will consider this case first and then extend the results to account for the effects of finite bandwidth. For the three discriminators described earlier, the thermal noise tracking error variance is as follows:

Coherent

$$\sigma_\tau^2 \approx \frac{B_L d}{2\mathrm{C/N_0}} \tag{17}$$

Early-minus-late power

$$\sigma_\tau^2 = \frac{B_L d}{2\mathrm{C/N_0}}\left[1+\frac{2}{T(2-d)\mathrm{C/N_0}}\right] \tag{18}$$

Dot-product

$$\sigma_\tau^2 = \frac{B_L d}{2\mathrm{C/N_0}}\left[1+\frac{1}{(T)\mathrm{C/N_0}}\right] \tag{19}$$

where σ_τ^2 is the tracking error variance in units of prn chips squared, B_L is the code tracking loop bandwidth in Hz, d is the early-to-late correlator spacing normalized with respect to one chip (d is thus dimensionless and, for example, is equal to 0.5 if the early-to-late correlator spacing is 1/2 chip), $\mathrm{C/N_0}$ is the carrier-to-noise value in units of ratio-Hz, and T is the predetection integration interval in units of seconds. As mentioned earlier, for GPS the predetection integration interval is usually the period of a navigation data bit: 1/50 s. The term in brackets is the so-called "squaring loss" inherent in noncoherent DLL's. A plot of tracking error versus carrier-to-noise ratio for the three discriminators is given in Fig. 10. The rms error ranges from approximately 0.001 chip at high $\mathrm{C/N_0}$ to 0.1 chip for low $\mathrm{C/N_0}$. With the C/A-code chip being approximately 293 m, the errors thus range from 0.3–30 m. For GPS, $\mathrm{C/N_0}$ typically is higher than 35 dB-Hz, and so tracking errors generally run on the lower end of the range.

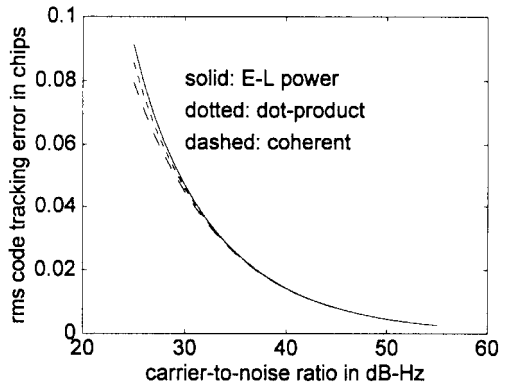

(a)

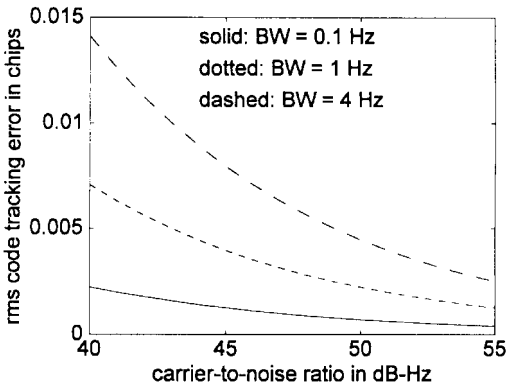

(b)

Fig. 10. RMS code tracking error due to noise. The correlator spacing, d, has been set to one (chip) and the predetection integration interval, T, has been set to 20 ms. In (a), the tracking loop bandwidth has been set to 4 Hz. At low $\mathrm{C/N_0}$ (i.e., below 35 dB-Hz), the coherent discriminator results are worse than are shown here due to excessive navigation bit errors. This portion ($<$35 dB-Hz) of the coherent plot is shown here for comparison purposes only. In (b), the coherent loop performance is plotted for three different tracking loop bandwidths.

Several points must be noted in order to interpret these equations and plots properly. In the presence of strong signals, all three discriminators converge to the same performance. The equation for the coherent discriminator is not valid at low carrier-to-noise ratios due to high navigation bit error rate. Also not described in the equations are the limits inherent in decreased correlator spacing. Although the equations indicate that tracking error tends to zero with decreasing correlator spacing, this is not actually true. The critical point is that the equations assume infinite signal bandwidth. In reality, the signal broadcast from the GPS satellite is limited approximately to a 30-MHz two-sided

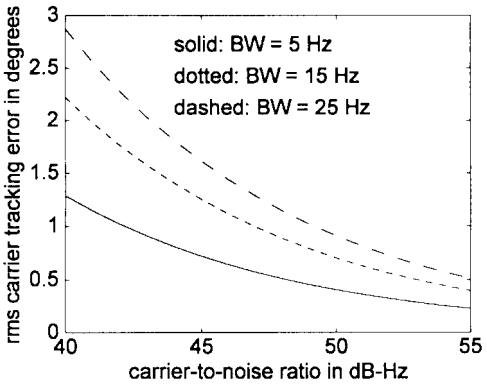

Fig. 11. RMS carrier-phase tracking error due to noise for three different carrier tracking loop bandwidths. The predetection integration interval T has been set to 20 ms.

bandwidth, and this is usually further reduced through receiver front-end filtering.

Although closed-form expressions do not exist, Van Nee [22] has determined the limitations inherent in the finite-bandwidth signals. The primary limitation is a bound in the noise reduction achieved with decreasing correlator spacing. Van Nee has defined a noise reduction factor as the ratio of the rms tracking error for infinite bandwidth and one-chip correlator spacing to that of the rms error for finite bandwidth and arbitrary correlator spacing less than or equal to one chip. It has been shown that for a receiver front-end bandwidth of k/Tc, the noise reduction factor converges for correlator spacings of $1/k$ or less (Tc is the prn chipping period and thus k/Tc is equal to k times the first-null bandwidth). For example, consider a GPS receiver with a front-end bandwidth of approximately 8 MHz. This is approximately eight times $1/Tc$, $Tc = 1/1.023 \times 10^6$ [s]. The aforementioned parameter k is thus equal to eight. As a result, maximum noise reduction is achieved for all correlator spacings of 1/8 chip or less. For this particular case, numerical evaluation shows the noise reduction factor to be approximately 7 [22]. This 1/8 chip "narrow correlator" receiver architecture thus achieves a factor of seven reduction in noise over the infinite bandwidth, one-chip correlator receiver.

Turning attention now to the carrier tracking loop, the PLL is implemented in the form of a Costas loop and the tracking error variance can be approximated by [10], [16]

$$\sigma_\theta^2 = \frac{\mathrm{B}_L}{\mathrm{C/N_0}}\left[1 + \frac{1}{(2T)\mathrm{C/N_0}}\right] \tag{20}$$

where σ_θ^2 is given in radians-squared, B_L is the carrier tracking loop bandwidth in Hz, $\mathrm{C/N_0}$ is the carrier-to-noise value in ratio-Hz, and T is the predetection integration interval in seconds. A plot of the rms tracking error as a function of carrier-to-noise ratio for several loop bandwidths is given in Fig. 11. In the range of $\mathrm{C/N_0}$ given (40–55 dB-Hz), the rms tracking error ranges from 3° down to 0.5°. For the L1 carrier (wavelength is approximately 0.19 m), the error thus ranges from 1.6 mm down to 0.3 mm.

The tracking error thus is directly proportional to the loop bandwidth and inversely proportional to the signal strength and predetection integration interval. For the nominal range of carrier-to-noise ratios, 35 dB-Hz and above, the second term in parentheses, known as the squaring loss, is negligible. It is important to recognize the tracking error expression is valid regardless of the tracking loop order so long as the loop gain is small enough not to cause stability problems. The choice of loop order is driven by dynamics, not noise performance.

After analyzing the tracking error equations, one might be tempted to improve code noise performance by narrowing the loop bandwidth. However, there is a price to pay and that price is dynamic performance. In the absence of any kind of aiding, receivers which experience significant accelerations, such as aircraft, must employ wider bandwidths and/or higher order tracking loops than stationary receivers, such as surveying units. In addition, local oscillator phase noise limits the lower bound on tracking loop bandwidth even for stationary receivers. For GPS, unaided code tracking loop bandwidths typically are on the order of a few Hertz and unaided carrier tracking loop bandwidths are in the range of 5–15 Hz.

One way to improve both noise and dynamic tracking performance simultaneously in code tracking loops is to employ rate-aiding. Since the carrier-tracking accuracy is excellent even at wide bandwidths (see Fig. 11), its velocity measurements can be used to aid the code-tracking loop. This can be performed in two ways. The first way is to make the aiding an integral part of the code loop in which case it is referred to as carrier-aiding. If the carrier loop measurements are used to aid the code loop, the code tracking loop bandwidth may be narrowed without suffering significant lags during signal dynamics. The second technique is to use the integrated Doppler measurements as a trajectory reference against which to smooth the noise in the pseudo-range measurements. This technique is referred to as carrier-smoothing [8]. Although the aforementioned has focused on aiding the code loop, it is also possible to derive similar benefits in the carrier loop. Rate aiding of the carrier loop can be achieved through integration of the GPS receiver with an inertial measurement unit.

In accord with sampling theory, the maximum independent sampling rate is twice the tracking loop bandwidth. As mentioned earlier, unaided code tracking loops have bandwidths on the order of 1–4 Hz depending upon the expected dynamics. This gives rise to maximum sampling rates of 2–8 Hz. GPS PLL's, however, generally operate with tracking loop bandwidths in the range of 5–15 Hz, thus providing data rates of 10–30 Hz. Most receivers, however, provide outputs ranging from 1–10 Hz. This addresses the need (in current receivers) to minimize the burden on the internal bus structure and the processor throughput capability. Data latency is a related issue which is also governed primarily by internal communication and processor capabilities. Typical latencies range from 200 ms to 2 s.

2) Interference Performance: Although interference, typically in the form of jamming, is of primary concern to the military user, civil users are also impacted by interference. The primary civil concern is that of unintentional interference as a result of harmonics, spurious emissions, or intermodulation products from non-GPS transmitters which fall in the GPS bands. Safety critical applications such as civil aviation have spurred a variety of tests and theoretical analyses [23]–[25]. The majority of high level interference has been observed on the European continent [26]. In particular, amateur radio digital data transmitters (packet-radio transmitters or digipeaters) operating at approximately 1240 MHz have been observed to cause complete blockage of the L2 signal [26].

The exact impact of interference is dependent both on the interference type and the GPS receiver architecture. Both subjects are treated theoretically in [27] and [28]. Narrowband interference resistance is inherent in direct sequence spread spectrum systems. A typical GPS C/A-code receiver can tolerate a narrow band interferer that is approximately 40 dB stronger than the GPS signal. This is referred to as interference-to-signal ratio (I/S) or jammer-to-signal ratio (J/S). The key weakness with the C/A-code is its relatively short period. With a period of 1 ms, the C/A-code spectrum is not continuous, but rather it is a line spectrum. If a narrowband interferer jams a strong C/A-code line, additional degradation will result.

As Ward [28] has pointed out, a receiver's ability to tolerate I/S equal to 40 dB sounds impressive until the absolute interference power is calculated. With a minimum received signal power of approximately -160 dBW, the interference need only be stronger than 1 pW to disable the receiver. In field tests, 1-W jammers have been shown to disable civilian receivers over more than a 20-km radius. Recent bench tests have shown that high-end receivers can experience position errors on the order of ten meters just prior to loss of lock when operating in the presence of broadband noise [25]. For the sake of completeness, it should be pointed out that there was no loss of integrity in this bench test. The C/N_0 computed by the receiver accurately reflected the strong noise environment.

Narrowband filtering in the front end is commonly employed to reduce the receiver's susceptibility to out-of-band interference. The most dramatic impact of receiver design on interference performance, however, can be observed when narrow band interference is considered.

The key issue is the fact that a sinusoid spends very little time near zero. Instead, it spends most of its time near its peak positive and negative values. Now consider a GPS receiver with a 1-bit sampling architecture. As long as the sinusoidal interferer is stronger than the GPS signal, the 1-bit A/D converter will be captured by the sinusoid. In other words, the GPS signal is dithering the sinusoid but the A/D converter cannot observe this. On the other hand, in a multibit architecture with adaptive thresholds, the thresholds can be set close to the peak positive and negative received signal values and thus can observe the GPS-induced dither [27], [29].

3) Multipath Performance: As with interference, multipath is generated external to the receiver, yet the receiver architecture has a significant impact on performance. The primary multipath parameters are strength, delay, phase, and phase-rate, all measured relative to the direct signal. The relative multipath strength is denoted as the multipath-to-direct ratio (M/D). As with thermal noise, analysis of the code and carrier tracking loops yield the relationship between the multipath parameters and the resulting measurement errors [22], [30]–[36], [43].

Conceptually, the effect of multipath on the pseudorange and carrier-phase measurements may be understood as follows. First, consider the discriminator functions plotted in Fig. 12 (recall Fig. 4 shows how the discriminator is formed from the early and late correlation functions). Fig. 12(a) shows a coherent discriminator for a received signal consisting of the direct ray only. Now consider a single multipath ray which is in-phase and distorting the direct signal. The resulting discriminator function is plotted in Fig. 12(b). Analytically, this may be considered as the sum of two discriminator components. One is associated with the direct signal and the other is associated with the multipath [Fig. 12(c)]. As discussed earlier, the code tracking loop adjusts the locally generated code such that the discriminator output is forced to zero. In the presence of multipath [Fig. 12(b)], however, the zero-crossing is shifted from the correct position [Fig. 12(a)]. This results in the local code lagging or leading the received direct code. The pseudorange multipath error is thus given by the amount of lag or lead in the local code.

In the presence of a single multipath ray, the pseudorange multipath error envelope is plotted in Fig. 13 [32]. The initial slope is a function of multipath amplitude and delay only. This initial slope thus is independent of correlator spacing and prn chipping rate. If the multipath delay is "short," the resulting pseudorange error will be the same for C/A-code or P-code. Another item to note is the presence of error at long delays resulting from the nonzero prn code autocorrelation sidelobes.

For multipath weaker than the direct signal and a correlator spacing of one chip, the maximum error is one-half chip. This is approximately 147 m for the C/A-code and 14.7 m for the P-code. As was the case for the noise equations, the multipath theory assumes infinite GPS signal bandwidth. Finite bandwidth effects can be handled through simulation and the results are similar to those of the infinite bandwidth case [21], [34]. The finite bandwidth effects are most apparent at medium and long delays with errors increasing by 20% to 40% over the infinite bandwidth case. For short delay multipath, the finite bandwidth effects are much less significant.

Similar to the noise case, multipath performance is also improved with narrow correlator architectures. The peak error (Fig. 13) is scaled by the correlator spacing d. It follows, then, that a narrow correlator receiver with $d = 0.1$ would experience a maximum pseudorange error of 14.7 m, whereas a standard correlator ($d = 1$) receiver would experience 147 m of error. Since the error given

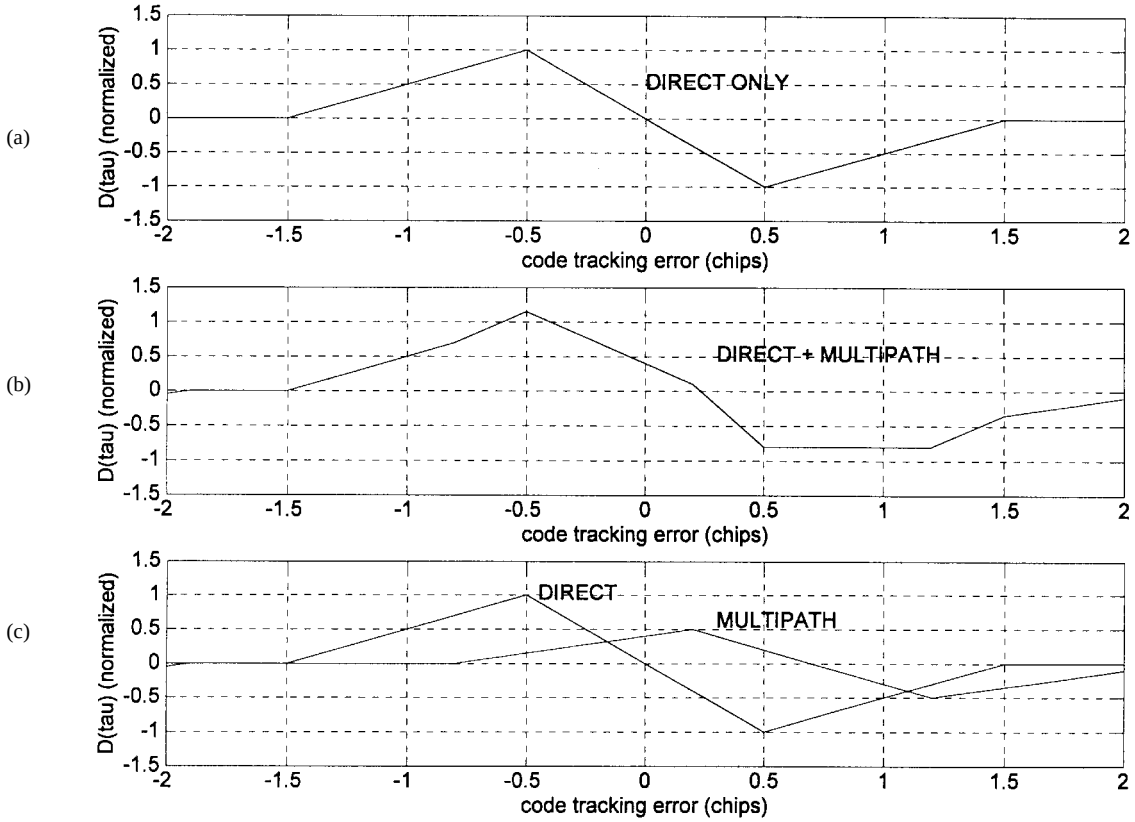

Fig. 12. Discriminator functions associated with (a) the direct signal only, (b) direct plus multipath signal, and (c) the direct-only component and the multipath-only component.

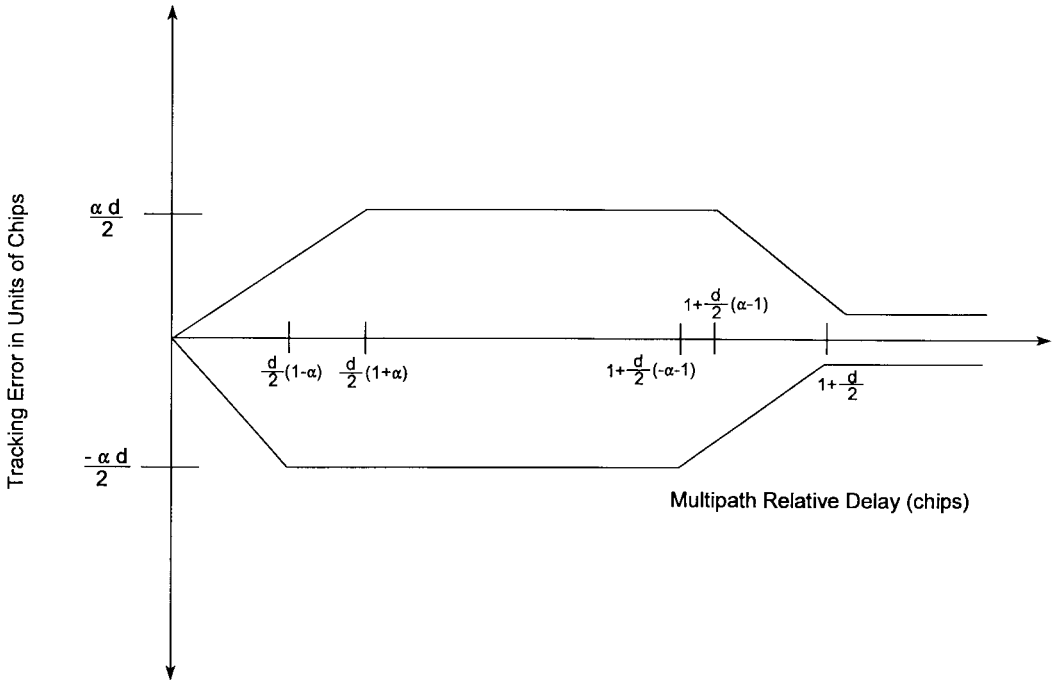

Fig. 13. Theoretical pseudorange multipath error envelope for the case of infinite signal bandwidth. The upper curve represents the case where the multipath is in-phase with the direct signal. The lower curve represents the out-of-phase case. In general, the actual multipath error will vary between these two extremes. The multipath-to-direct signal strength ratio is given by α and d is the early-to-late correlator spacing in units of prn chips. α is assumed to be less than one.

in Fig. 13 is in units of prn chips, one may conclude that P-code performance on the whole is better than for the C/A-code. This follows since a P-code chip is 1/10 the length of a C/A-code chip. In addition, the error envelope essentially goes to zero for delays greater than $1 + d/2$ chips since the P-code autocorrelation sidelobes are essentially negligible. The key exception to the superior P-code performance is in the case of short delay multipath (i.e., multipath with delays less than 1/10 C/A-chip length). As described in [33], all current receiver architectures have similar multipath performance in the presence of short delay multipath. In addition, recent developments in C/A-code receiver technology have improved medium and long delay multipath performance significantly. This improved multipath performance, however, is achieved at the price of loss of SNR and/or increased architecture complexity [37]–[42].

The effect of multipath on the carrier phase may be viewed most effectively through a phasor diagram (Fig. 14). The relative phase between the direct and multipath signal is denoted by θ_m. The receiver cannot distinguish the components of the distorted signal and thus must track the composite. The phase difference between the direct and composite signals θ_c is the carrier-phase multipath error. In order to determine an upper bound, it is assumed the relative phase-rate between the direct and multipath signal is zero. As a result, the $e^{j\omega t}$ time dependence relating the phasors to the actual time-domain signals can be ignored. The magnitudes of the direct and multipath phasors are given by

$$D = R(\tau) \tag{21}$$

$$M = \alpha R(\tau - \delta) \tag{22}$$

where $R(\tau)$ is the prn code autocorrelation function as a function of lag τ, δ is the delay of the multipath relative to the direct, and α is the ratio of the multipath signal strength to direct signal strength. α is sometimes referred to as multipath-to-direct ratio (M/D). In order to derive the equation for θ_c, it is convenient to decompose the multipath phasor into its in-phase (M_I) and quadrature (M_Q) components [Fig. 14(b)]. It is now apparent

$$\theta_c = \arctan\left(\frac{M_Q}{D + M_I}\right) \tag{23}$$

which may also be written

$$\theta_c = \arctan\left(\frac{\alpha R(\tau - \delta)\sin(\theta_m)}{R(\tau) + \alpha R(\tau - \delta)\cos(\theta_m)}\right). \tag{24}$$

The maximum possible error is $\pi/2$ radians or one-quarter carrier wavelength. For the GPS L1 frequency, this amounts to approximately 4.8 cm. This extreme is not common, however, and errors typically are less than 1 cm.

Recent developments in receiver architectures have achieved some reduction in carrier-phase multipath error [22], [37], [40], [42]. As with the pseudorange improvements, the carrier-phase improvement is achieved only for medium and long-delay multipath. Of the three techniques proposed [37], [40], [42], only one has been documented publicly [22], [37]. Theoretical performance and field trial results have been published for the other two but the implementation details so far have not been made public.

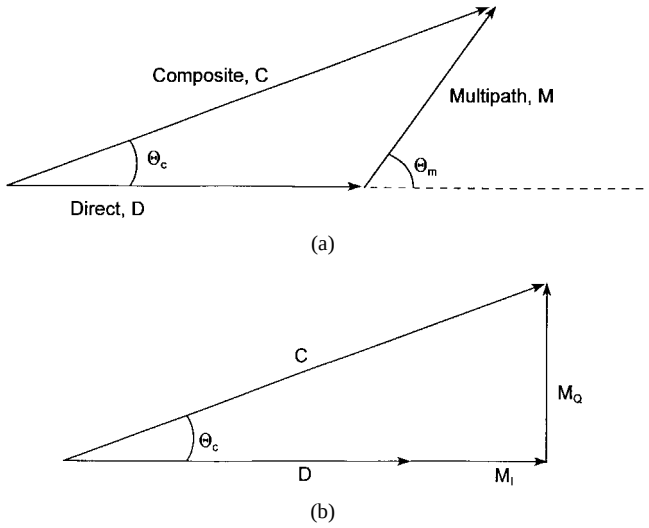

Fig. 14. Phasor diagram depicting relationship between relative multipath strength, phase (θ_m), and resulting carrier phase error. In (a) the composite received signal is shown to be the vector sum of the direct plus multipath. The phase difference between the direct and the composite is the carrier-phase multipath error (θ_c). In (b) the multipath phasor is decomposed into its in-phase and quadrature components for the purpose of deriving the equation for the arctangent of θ_c.

To conclude this section we recall the C/A-code pseudorange multipath error can approach 147 m, theoretically. As long as the receiver is not in the vicinity of large obstacles, however, errors of 10 m or less are far more common. Large errors can be encountered in the urban environment, specifically near skyscrapers. Pseudorange errors in excess of 100 m have been measured with stationary GPS receivers located near skyscrapers [22]. This is of particular concern in applications such as vehicle navigation systems.

V. Conclusions

This paper has provided an overview of the processing performed in a GPS receiver and the various tradeoffs possible in the design. Currently, the cost of a GPS receiver (*not* in quantity) ranges from approximately \$100–\$20 000. Performance roughly parallels cost. High-end receivers are marked by low-noise front ends, multibit A/D converters, and higher speed digital signal processing. This, in turn, allows for noise, multipath, and interference reduction. In addition, high-end civilian receivers are available which track both GPS frequencies. As more receivers are manufactured in high volume ASIC-based designs, it is expected that even high performance will be available at lower prices.

As was stated in the introduction, GPS is being utilized in a wide variety of civilian applications. For example, a high-end survey receiver will track both GPS frequencies through an extremely low-noise front end and narrow carrier tracking loops. This allows for the highest precision

possible in the carrier phase measurements. Dynamics are not a problem for the narrow tracking loop since the receiver will not undergo significant dynamics. In addition, it is not uncommon for survey receivers to have data latencies on the order of a second. Again, this is perfectly acceptable since the receiver typically is experiencing low dynamics and the data is not being used in real time.

The GPS receiver found in a transoceanic aircraft will be quite different than a survey receiver. With safety-of-life as the primary issue, reliability and availability are as important as accuracy. The receiver must operate in a wide variety of environmental conditions including interference. Acceptable interference performance may require narrowband front-end filters, multibit adaptive A/D converters, and subsequent complex baseband processing. Operation at low C/N_0 may require noncoherent carrier and code loop mechanizations. These loops exhibit wider hold-in ranges but pay the price with slightly degraded tracking accuracy.

The wide variety of applications is a testimony to the utility of the system. Receiver manufacturers have met this challenge with an equally wide variety of receiver architectures. Equipment buyers must be aware of the aforementioned differences and must be careful to match the receiver performance specification to the requirements of the given application.

REFERENCES

[1] R. Ziemer and R. Peterson, *Digital Communications and Spread Spectrum Systems.* New York: Macmillan, 1985.

[2] ——, *Introduction to Digital Communication.* New York: Macmillan, 1992.

[3] R. Gold, "Optimal binary sequences for spread spectrum multiplexing," *IEEE Trans. Inform. Theory*, vol. IT-13, pp. 619–621, Oct. 1967.

[4] J. J. Spilker, Jr., "GPS signal structure and performance characteristics," *Navigation: J. Inst. Navigation*, vol. 25, no. 2, pp. 121–146, Summer 1978.

[5] ——, "GPS signal structure and theoretical performance," in *Global Positioning System: Theory and Application*, vol. I, B. W. Parkinson and J. J. Spilker, Jr., Eds. Washington, DC: American Institute of Aeronautics and Astronautics, 1996, ch. 3, pp. 57–120.

[6] P. Misra, B. P. Burke, and M. M. Pratt, "GPS performance in navigation," this issue, pp. 65–85.

[7] T. A. Herring, "Geodetic applications of GPS," this issue, pp. 92–110.

[8] R. Hatch, "Synergism of GPS code and carrier measurements," in *Proc. 3rd Int. Geodetic Symp. Satellite Doppler Positioning*, Feb. 1982, pp. 1213–1232.

[9] M. Bailey, "A broad-beam circularly-polarized antenna," in *Dig. IEEE Antennas and Propagation Society (AP-S) Int. Symp.*, Stanford University, Stanford, CA, June 1977, pp. 238–241.

[10] A. J. Van Dierendonck, "GPS receivers," in *Global Positioning System: Theory and Application*, vol. I, B. W. Parkinson and J. J. Spilker, Jr., Eds. Washington, DC: American Institute of Aeronautics and Astronautics, 1996, ch. 8, pp. 329–407.

[11] M. Braasch and F. van Graas, "Guidance accuracy considerations for realtime GPS interferometry," in *Proc. 4th Int. Tech. Meeting Satellite Division of the Institute of Navigation*, Sept. 1991, pp. 373–386.

[12] P. Nieuwjaar, "GPS signal structure," NATO AGARD Lecture Series No. 161, The NAVSTAR GPS System, Sept. 1988.

[13] S. C. Fisher and K. Ghassemi, "GPS IIF—The next generation," this issue, pp. 24–47.

[14] Anonymous, Interface Control Document ICD-GPS-200, Arinc Research Corporation, Fountain Valley, CA, July 1991.

[15] D. Akos, "A software radio approach to global navigation satellite system receiver design," Ph.D. dissertation, School of Elect. Eng. Comput. Sci., Ohio Univ., Athens, OH, Aug. 1997.

[16] P. Ward, "Satellite signal acquisition and tracking," in *Understanding GPS: Principles and Applications*, E. Kaplan, Ed. Boston: Artech House, 1996, ch. 5, pp. 119–208.

[17] R. Hatch, R. Keegan, and T. Stansell, "Kinematic receiver technology from Magnavox," in *Proc. 6th Int. Geodetic Symp.*, Mar. 1992.

[18] A. J. Van Dierendonck, "Understanding GPS receiver terminology: A tutorial on what those words mean," in *Proc. Int. Symp. Kinematic Syst.*, Sept. 1994, pp. 15–24.

[19] S. Gourevitch and J. Nolan, "Tracking results: Implications to precision civilian applications," in *Proc. 6th Int. Tech. Meeting Satellite Division of the Institute of Navigation*, Sept. 1993, pp. 1021–1025.

[20] P. Enge, "The global positioning system: Signals, measurements, and performance," *Int. J. Wireless Inform. Networks*, vol. 1, no. 2, pp. 83–105, 1994.

[21] A. J. Van Dierendonck, P. Fenton, and T. Ford, "Theory and performance of narrow correlator spacing in a GPS receiver," *Navigation: J. Inst. Navigation*, vol. 39, no. 3, pp. 265–283, Fall 1992.

[22] R. Van Nee, "Multipath and multi-transmitter interference in spread-spectrum communication and navigation systems," Ph.D. dissertation, Faculty Elect. Eng., Delft Univ. Technol., Delft, The Netherlands, 1995.

[23] C. Hegarty, "Analytical derivation of maximum tolerable in-band interference levels for aviation applications of GNSS," *Navigation: J. Inst. Navigation*, vol. 44, no. 1, pp. 25–34, Summer 1997.

[24] B. Schnaufer and G. McGraw, "WAAS receiver carrier tracking loop and data demodulation performance in the presence of wideband interference," *Navigation: J. Inst. Navigation*, vol. 44, no. 1, pp. 35–42, Summer 1997.

[25] T. Skidmore and F. Liu, "WAAS/LAAS interference test results," in *Proc. Inst. Navigation National Tech. Meeting*, Santa Monica, CA, Jan. 1997, pp. 839–848.

[26] F. Butsch, "GPS interference problems in Germany," in *Proc. Inst. Navigation Annu. Meeting*, Albuquerque, NM, June 1997, pp. 59–67.

[27] J. Spilker, Jr. and F. Natali, "Interference effects and mitigation techniques," in *Global Positioning System: Theory and Application*, vol. I, B. W. Parkinson and J. J. Spilker, Jr., Eds. Washington, DC: American Institute of Aeronautics and Astronautics, 1996, ch. 20, pp. 717–771.

[28] P. Ward, "Effects of RF interference on GPS satellite signal receiver tracking," in *Understanding GPS: Principles and Applications*, E. Kaplan, Ed. Boston: Artech House, 1996, ch. 6, pp. 209–236.

[29] F. Amoroso, "Adaptive A/D converter to suppress CW interference in DSPN spread-spectrum communications," *IEEE Trans. Commun.*, vol. COM-31, pp. 1117–1123, Oct. 1983.

[30] L. Hagerman, "Effects of multipath on coherent and noncoherent PRN ranging receiver," Development Planning Division, The Aerospace Corporation, Report TOR-0073(3020-03)-3, May 1973.

[31] R. Van Nee, "Spread spectrum code and carrier synchronization errors caused by multipath and interference," *IEEE Trans. Aerospace Electron. Syst.*, vol. 29, pp. 1359–1365, Oct. 1993.

[32] M. Braasch, "Autocorrelation sidelobe considerations in the characterization of multipath errors," *IEEE Trans. Aerospace Electron. Syst.*, vol. 33, pp. 290–295, Jan. 1997.

[33] ——, "GPS multipath model validation," in *Proc. IEEE Position, Location, and Navigation Symp.*, Apr. 1996, pp. 672–678.

[34] G. Brodin, "GNSS code and carrier tracking in the presence of multipath," in *Proc. ION GPS-96*, p. 1389.

[35] M. Braasch, "On the characterization of multipath errors in satellite-based precision approach and landing systems," Ph.D. dissertation, School of Elect. Eng. Comput. Sci., Ohio University, Athens, OH, June 1992.

[36] ——, "Multipath effects," in *Global Positioning System: Theory and Application*, vol. I, B. W. Parkinson and J. J. Spilker, Jr., Eds. Washington, DC: American Institute of Aeronautics and Astronautics, 1996, ch. 14, pp. 547–568.

[37] R. Van Nee, J. Siereveld, P. Fenton, and B. Townsend, "The multipath estimating delay lock loop: Approaching theoretical accuracy limits," in *Proc. IEEE Position, Location, and Navigation Symp.*, Apr. 1994, pp. 246–251.

[38] A. J. Van Dierendonck and M. Braasch, "Evaluation of GNSS receiver correlation processing techniques for multipath and noise mitigation," in *Proc. Institute of Navigation Nat. Tech. Meeting*, Jan. 1997, pp. 207–215.
[39] L. Weil, "GPS multipath mitigation by means of correlator reference waveform design," in *Proc. Institute of Navigation Nat. Tech. Meeting*, Jan. 1997, pp. 197–206.
[40] R. Hatch, R. Keegan, and T. Stansell, "Leica's code and phase multipath mitigation techniques," in *Proc. Institute of Navigation Nat. Tech. Meeting*, Jan. 1997, pp. 217–225.
[41] L. Garin, F. Van Diggelen, and J. Rousseau, "Strobe and edge correlator multipath mitigation for code," in *Proc. 9th Int. Tech. Meeting Satellite Division of the Institute of Navigation*, Sept. 1996, pp. 657–664.
[42] L. Garin and J. Rousseau, "Enhanced strobe correlator multipath rejection for code and carrier," in *Proc. 10th Int. Meeting Satellite Division of the Institute of Navigation*, ION GPS-97, Kansas City, MO, Sept. 1997, pp. 559–568.
[43] P. Enge, "Local area augmentation of GPS for the precision approach of aircraft," this issue, pp. 111–132.
[44] C. C. Counselman, III "Multipath-rejecting GPS antennas," this issue, pp. 86–91.

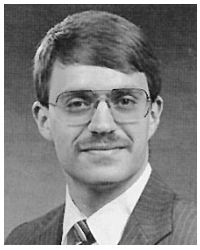

Michael S. Braasch (Member, IEEE) received the Ph.D. degree in electrical engineering from Ohio University, Athens, in 1992.

He has been performing research with the Avionics Engineering Center at Ohio University since 1985 and has worked on a variety of aircraft navigation systems including ILS, MLS, VOR, Loran-C, DME, INS, and GPS. In 1993, he served as a Visiting Scientist at the Delft University of Technology in the Netherlands. Since 1994, he has been an Assistant Professor in the School of Electrical Engineering and Computer Science and a Research Scientist with the Avionics Engineering Center, Ohio University. He has lectured for NATO AGARD and has authored book chapters on multipath and selective availability. Since 1995, he has directed the GPS software radio and signal modeling research teams at Ohio University.

Dr. Braasch has supported the FAA in national and international forums such as RTCA, the ICAO All Weather Operations Panel, and the ICAO Obstacle Clearance Panel. In 1992, his dissertation characterizing the effects of multipath on DGPS landing systems won the RTCA's William E. Jackson Award for an outstanding publication in aviation electronics.

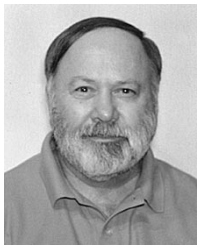

A. J. Van Dierendonck (Senior Member, IEEE) received the B.S.E.E. degree from South Dakota State University, Vermillion, and the M.S.E.E. and Ph.D. degrees from the Iowa State University, Iowa City.

He has 25 years of GPS experience. Currently, he is self-employed under the name of AJ Systems and is a General Partner of GPS Silicon Valley.

In 1993, Dr. Van Dierendonck was awarded the Johannes Kepler Award by the Institute of Navigation Satellite Navigation Division for outstanding contributions to satellite navigation. In 1997, he was awarded the ION Thurlow Award for outstanding contributions to the science of navigation.